The Bioscan
AN INTERNATIONAL QUARTERLY JOURNAL OF LIFE SCIENCES
20(4): 1308-1333, 2025 www.thebioscan.com

Design of Hybrid Adaptive Fractional Order Model with Multi-Criteria Objective Function for Enhanced Mammographic Image Segmentation in Breast Cancer Detection

J Jansi Rani[1*], RajaKumar T.C[2]

[1]Research Scholar, (Reg. No. 21121282282020), PG & Research Department of Computer Science, St. Xavier's College (Autonomous), Palayamkottai, Affiliated to Manonmaniam Sundaranar University, Abishekapatti, Tirunelveli-627012. E-mail: jjansirani205@gmail.com

[2]Associate Professor, PG & Research Department of Computer Science, St. Xavier's College (Autonomous), Palayamkottai, Affiliated to Manonmaniam Sundaranar University, Abishekapatti, Tirunelveli-627012. E-mail: grajazion@gmail.com

DOI: 10.63001/tbs.2025.v20.i04.pp1308-1333

KEYWORDS
Hybrid adaptive fractional-order DPSO framework,multi-criteria objective function,Mammographic image Segmentation,Breast Cancer Detection,Dynamic Particle Swarm Optimisation.

Received on:

18-09-2025

Accepted on:

14-11-2025

Published on:

17-12-2025

ABSTRACT

This paper presents a hybrid adaptive fractional-order DPSO framework for multi-threshold mammographic image segmentation that aims to enhance the delineation of dense tissue and abnormalities at their early stage. The method incorporates a multi-criteria objective function combining between-class variance, edge alignment and inter-channel coherence to enhance statistical separability and structural accuracy. It also utilizes adaptive scheduling of the inertia and acceleration coefficients for balancing exploration and exploitation during optimization and fractional-order velocity updates to introduce long-term memory for smoother and more stable convergence. The proposed framework is qualitatively and quantitatively evaluated using the Mini-MIAS dataset, considering improvements in segmentation accuracy, boundary preservation, convergence speed and consistency in comparison with Otsu's thresholding, classical PSO and standard DPSO. Confirmatory experiments in both grayscale and perceptually uniform colour spaces reinforce the model's capabilities in delivering coherent and clinically meaningful segmentations. The proposed approach lays a sound foundation for optimization-driven mammogram analysis and future computer-aided detection systems.

I. Introduction

Despite being one of the most serious health concerns for women globally, early diagnosis remains the only way to help reduce mortality burdens due to breast cancer [1]. Mammography remains a critical modality in both screening and diagnosis, allowing radiologists to noninvasively detect abnormalities at the earliest stages. Indeed, mammograms are images with complex characteristics due to the presence of an overlay of tissue density,

low-contrast areas and subtle lesion borders, which make correct interpretations challenging [2]. Image segmentation is a basic step in automatic mammogram analysis, since the goal is to delimitate regions of interest that could enhance visibility for diagnoses [3]. However, traditional thresholding methods such as Otsu's technique, entropy-based thresholding and region-based methods depend highly on histogram statistics, presuming well-separated distributions of intensity. Naturally, mammographic images are inherently multimodal, so dense, fatty and abnormal tissues can be overlapped in intensity, causing a limitation of traditional segmentation techniques.Recent developments in computational intelligence have enabled optimization-based segmentation models [4], notably PSO and its dynamic variants. The PSO-based multi-thresholding formulates the segmentation as a global optimization problem, which allows locating threshold values in complex histograms with multiple peaks, where classes are nonlinearly separable. Though simple and efficient, classical PSO suffers from premature convergence, loss of swarm diversity and stagnation in local optima, especially while dealing with large search spaces associated with multi-level thresholding [5]. Some of these limitations have been overcome by DPSO through adaptive adjustments of particles, but ensuring structural boundary preservation and perceptual consistency in the segmented outputs remains a challenge.

This research addresses this gap by proposing a hybrid multi-criteria objective function and an enhanced swarm mechanism aimed at bringing about improvement in segmentation precision, stability and perceptual coherence. In the proposed framework, we combine statistical, gradient-based and channel-consistency cues for guiding the optimization process toward meaningful threshold positions. Fractional-order swarm dynamics and adaptive parameter scheduling further enhance convergence behaviour by incorporating long-term memory into particle motion and balancing exploratory and exploitative phases during optimization [6].The research problem to be addressed in this work deals with the development of a robust, perceptually aware and structurally sensitive multi-threshold segmentation framework for mammographic images that overcomes the limitations of classical PSO-based methods to deliver clinically meaningful boundaries even when the imaging conditions are poor.

The objective of this research is to design a hybrid multi-criteria fitness function combining between-class variance, edge alignment and inter-channel coherence for improved segmentation quality. Later, the adaptive schedulingof inertia and acceleration coefficients are included for better convergence control. Fractional-order velocity updates are incorporated

into PSO/DPSO for enhancing stability and reducing susceptibility to local maxima. Finally, the proposed framework is evaluated on mammographic datasets and compare against baseline segmentation techniques.The scope of the study encompasses multi-threshold segmentation of grayscale and colour-space mammographic images, evaluation using quantitative and perceptual metrics and comparative analysis against existing optimization-based approaches. Research focuses only on the segmentation part and does not include a classification or clinical decision module.

II. Materials and Methods

The research focused on strengthening the segmentation framework by introducing hybrid multi-criteria optimisation, adaptive swarm control and fractional-order search dynamics. The aim of this research was to design a fitness landscape that accurately reflects structural, statistical and perceptual properties of mammographic images and to integrate swarm mechanisms capable of navigating this landscape without stagnation [7]. This section presents the materials used for the experiments and provides a detailed description of the mathematical derivations, objective formulation and optimisation strategies incorporated into the proposed framework.

2.1.Dataset and Pre-processing

Experiments in this research were performed using the Mini-MIAS mammogram database, a widely used benchmark for breast tissue analysis. Images from the dataset exhibit heterogeneous intensity distributions caused by the coexistence of fatty, glandular and dense tissues. This variability makes the dataset suitable for testing the ability of the proposed multi-criteria objective to handle multimodal histograms and low-contrast boundaries [8].Each mammogram was first normalized to the range [0, 255], followed by Gaussian smoothing to suppress film noise while retaining large-scale tissue structures. For colour-space experiments, the grayscale mammograms were converted into pseudo-colour representations by mapping them into the CIELAB and YCbCr spaces. These spaces were selected because they separate luminance and chrominance components and provide a perceptually uniform representation, which is essential for evaluating the inter-channel coherence term in the hybrid fitness function.

2.2.Hybrid Multi-criteria Fitness Function

The central contribution of this research is the introduction of a composite objective function that evaluates candidate thresholds using three complementary measures: statistical separability, edge conformity and inter-channel consistency. Let $T = \{t_1, t_2, \dots, t_m\}$denote a set of $m$thresholds produced by a swarm particle.The classical between-class variance for multi-threshold images is derived from Otsu's formulation. For an image with histogram $h(i)$and normalized probabilities$p(i) = h(i)/N$, the class probabilities and class mean for region $k$defined by thresholds $t_k$and $t_{k+1}$are given in Eq.1.

$$\omega_k = \sum_{i=t_k+1}^{t_{k+1}} p(i)\,, \mu_k = \frac{1}{\omega_k} \sum_{i=t_k+1}^{t_{k+1}} i\,p(i) \quad \text{Eq.1.}$$

The global mean is calculated as given in Eq.2.

$$\mu_T = \sum_{i=0}^{L-1} i\,p(i) \quad \text{Eq.2.}$$

The between-class variance is then computed as given in Eq.3.

$$F_{\text{var}}(T) = \sum_{k=0}^{m} \omega_k(\mu_k - \mu_T)^2 \quad \text{Eq.3.}$$

Maximizing F_{var}leads to threshold sets that best separate the histogram into statistically distinct regions corresponding to major anatomical components.Edge boundaries are critical for delineating lesions and dense tissue. The edge alignment [9] term incorporates gradient information by encouraging threshold placement at locations where the underlying intensity transitions are prominent. Let $E(x, y)$denote the edge magnitude obtained using Sobel or Canny operators. For each threshold t_j, the pixels whose intensities fall within a narrow band around the threshold are identified as given in Eq.4.

$$\Omega_j = \{(x, y) \mid\mid I(x, y) - t_j \mid \leq \delta\} \quad \text{Eq.4.}$$

The edge alignment score is calculated asderived in Eq.5.

$$F_{\text{edge}}(T) = \sum_{j=1}^{m} \frac{1}{|\Omega_j|} \sum_{(x,y)\in\Omega_j} E(x, y) \quad \text{Eq.5.}$$

Higher values of F_{edge}indicate that the thresholds are aligned with true anatomical boundaries, improving structural precision. In perceptual colour spaces, different channels represent distinct physiological or perceptual components. If thresholds vary excessively across channels, the segmented regions appear visually inconsistent [10]. To prevent such

artefacts, channel coherence is introduced. For a colour image with Cchannels and thresholds $T_c = \{t_1^c, t_2^c, \dots, t_m^c\}$, the coherence penalty is defined as given in Eq.6.

$$F_{\text{coh}} = \sum_{j=1}^{m} \sum_{c=1}^{C} \sum_{d=1,\ d\neq c}^{C} | t_j^c - t_j^d | \qquad \text{Eq.6.}$$

A small coherence value as given in Eq.6. corresponds to threshold alignment across luminance and chrominance components.The complete hybrid fitness function is expressed in Eq.7.

$$F(T) = \alpha F_{\text{var}}(T) + \beta F_{\text{edge}}(T) - \gamma F_{\text{coh}}(T) \qquad \text{Eq.7.}$$

where the weights α, $\beta$and γregulate the contribution of each term. Through empirical evaluation, the values were chosen such that variance dominated the early search while edge and coherence terms influenced fine-level refinement in later iterations. This formulation provides a balanced objective landscape that captures global statistics, local structure and perceptual coherence.

2.3.Adaptive PSO/DPSO Parameter Scheduling

To improve the convergence behaviour of the swarm [11] in this refined objective space, adaptive scheduling was applied to three parameters: inertia weight w, cognitive coefficient c_1 and social coefficient c_2. The inertia weight was gradually reduced from a high initial value $w_{\max}$to a lower bound $w_{\min}$ as given in Eq.8.

$$w(t) = w_{\min} + (w_{\max} - w_{\min})(1 - \frac{t}{T_{\max}}) \qquad \text{Eq.8.}$$

where $t$is the current iteration. High inertia in the initial stage enhances exploration, allowing particles to traverse the multimodal search space. As the iterations progress, the reduced inertia reduces oscillations and encourages exploitation.The acceleration coefficients were scheduled inversely as given in Eq.9 and Eq. 10.

$$c_1(t) = c_{1,\max} - (c_{1,\max} - c_{1,\min})\frac{t}{T_{\max}} \qquad \text{Eq.9.}$$

$$c_2(t) = c_{2,\min} + (c_{2,\max} - c_{2,\min})\frac{t}{T_{\max}} \qquad \text{Eq.10.}$$

Eq.9. and Eq.10. ensures that early iterations prioritize personal experience while later stages rely on collective experience for convergence.

2.4.Fractional-order Velocity Update

A major enhancement introduced in this research was the incorporation of fractional-order dynamics into the velocity update rule. Traditional PSO depends on the immediate previous velocity. Fractional calculus generalizes this behaviour by considering the influence of several past velocities with decaying non-integer weights. The fractional derivative of order $0 < \nu < 1$for velocity is approximated using the Grünwald–Letnikov formulation as given in Eq.11.

$$v_i^{(t)} = \sum_{k=0}^{t} \binom{\nu}{k} (-1)^k v_i^{(t-k)} + c_1 r_1 (p_i - x_i) + c_2 r_2 (g - x_i) \quad \text{Eq.11.}$$

where $\binom{\nu}{k}$represents generalized binomial coefficients. This mechanism gives the swarm a long-term memory that smoothens abrupt velocity changes, reduces oscillatory behaviour [12] and strengthens global search capability. Fractional dynamics also help the particles escape local traps created by sharp peaks in the hybrid fitness landscape. The overall optimisation workflow is depicted in Fig.1.

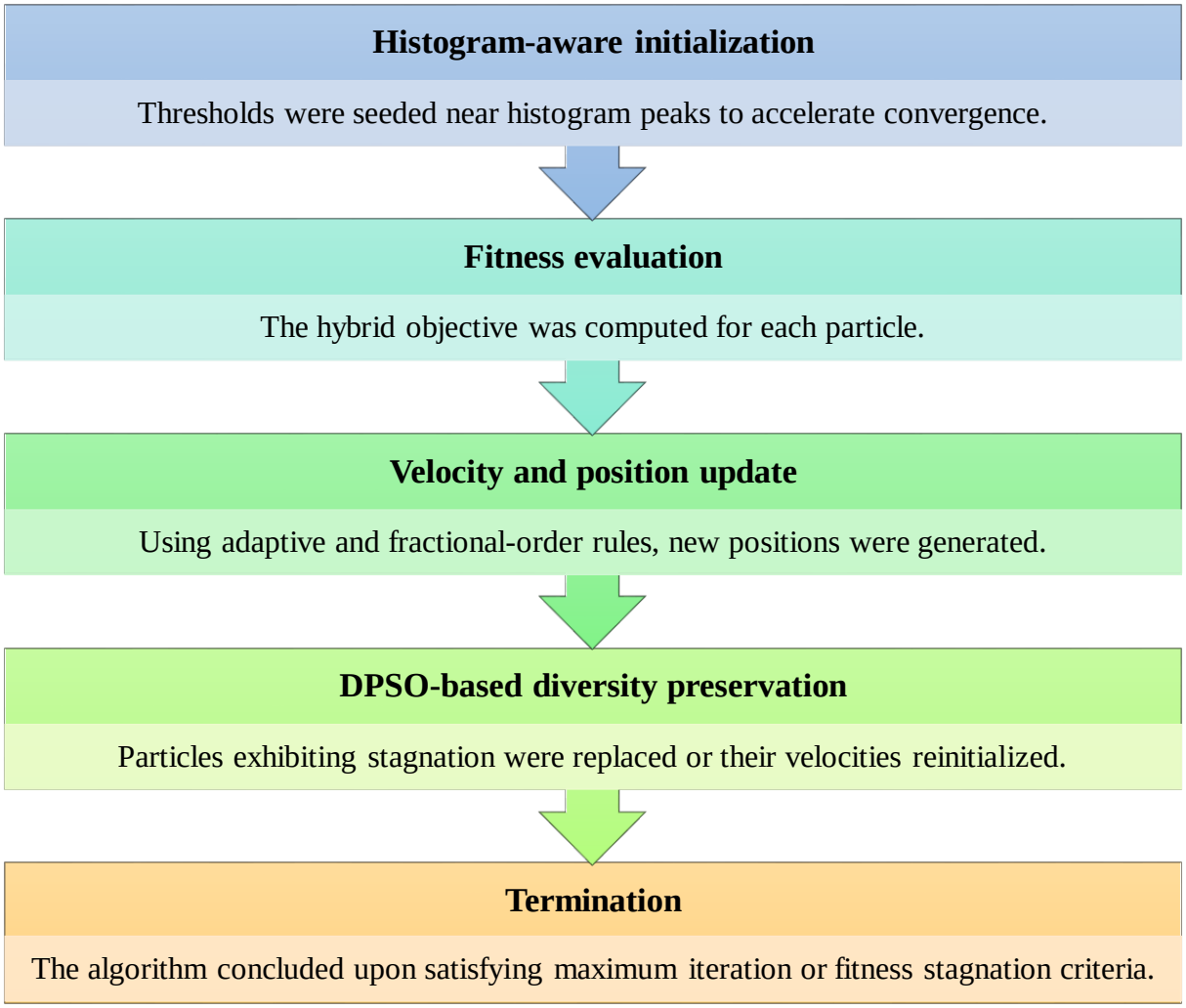

Fig.1. Optimisation Workflow of the proposed Hybrid model

Each particle in the swarm represented a vector of thresholds. For colour-space segmentation, channel-wise optimisation produced threshold sets for L*, a*, b* or Y, Cb, Cr channels. The final segmentation mask was obtained by majority fusion or weighted averaging depending on channel significance, ensuring perceptually consistent boundaries.

III. Experimentation and Implementation

This research work is designed to validate the developed hybrid multi-criteria segmentation framework of research by considering its performance under controlled conditions with mammographic images [13]. The implementation involves construction of the hybrid objective function, integrating adaptive and fractional swarm dynamics and conducting systematic experiments on convergence stability, boundary fidelity and perceptual coherence [14]. This section describes the entire implementation process, algorithmic workflow and experimental design adopted in this research of research.The core of the implementation was a hybrid fitness function. To construct it, a variance computation unit, an edge-alignment unit and a channel-coherence evaluation unit were developed as three independent modules. In order to maintain modularity and ensure weight adjustments at a fine-grain level, each module was implemented as an independent function [15].

This variance module computed between-class variance based on the thresholds proposed by each particle, operating on either grayscale or channel-specific intensities. The edge module used Sobel filtering to extract prominent boundaries. Edge magnitudes were pre-computed once per image to avoid redundancy and the alignment values were evaluated by mapping threshold neighbourhoods to gradient responses. The coherence module operated only when colour-space experiments were conducted: it would consume threshold vectors from L*, a*, b* or Y, Cb, Cr channels and compute the penalty associated with cross-channel threshold deviations.The three components were assembled in the weighted hybrid objective function as given in Eq.12.

$$F(T) = \alpha F_{\text{var}} + \beta F_{\text{edge}} - \gamma F_{\text{coh}} \quad \text{Eq.12.}$$

Eq.12. showed that with weight tuning performed empirically. Early experiments indicated that larger emphasis on between-class variance hindered the influence of the edge term, especially in mammograms with vague lesion boundaries. Thus, the weights were gradually adjusted until the resulting segmentations exhibited balanced statistical separation and

structural consistency [16].To exploit this newly built goal landscape, the swarm optimisation algorithm needed to steer particle behaviour dynamically. Three adaptive curves-inertia weight scheduling, cognitive coefficient scheduling and social coefficient scheduling-were integrated to extend the classical PSO formulation. These controls were implemented as time-varying functions that were evaluated at every iteration. At early iterations, the inertia was high and thus the particles could explore the fitness landscape widely. As iterations proceeded, the inertia was reduced and the social term became more dominant, enabling the swarm to converge collectively as promising regions were uncovered. This dynamic behaviour minimized early stagnation and made the optimization process sensitive to the multi-modal characteristics of mammographic image histograms. The integration of fractional-order dynamics [17] involved the use of memory-based velocity updates. A buffer that stored several previous velocities for each particle was allocated. The system employed the Grünwald-Letnikov approximation to merge these previous values using fractional binomial coefficients. This calculation was encapsulated inside the velocity update function. The fractional behaviour proved particularly useful during experiments involving complicated images featuring multiple transitions in tissue density. Naturally occurring local maxima in the objective landscape often misled the classical PSO; however, this fractional memory smoothed out abrupt changes and ushered the particles towards regions of persistently higher fitness.

The overall hybrid segmentation algorithm was a multi-staged procedure that involved various coordinated steps. Each of the stages was independently developed, although in the final implementation, the algorithm executed seamlessly. The steps of this hybrid algorithm are summarized below in narrative form. Start with loading any mammogram and do the pre-processing if needed, which includes noise smoothing, contrast enhancement, or colour space conversion, where applicable [18]. The intensity histogram is analysed and major peaks are automatically identified to initialize the particle thresholds close to meaningful tissue transitions. A swarm of particles was initialized, each containing a candidate threshold set. Velocity vectors were assigned randomly within pre-specified limits. For each iteration, the hybrid fitness function of all the particles was evaluated. Based on the resulting scores, update personal and global best thresholds. Then modify particle velocities through adaptive scheduling and fractional-order memory [19]. Re-initialize particles showing stagnation or regularly returning low performance to restore diversity. Update positions and sort thresholds to enforce feasibility. Repeat the loop until termination conditions were reached; typically,

best fitness stability or a maximum iteration count. The final thresholds were used to segment the images visually and then quantify. The overall algorithm for hybrid adaptive fractional-order DPSO framework is presented in Table.1.

Table.1. Algorithm for hybrid adaptive fractional-order DPSO framework

Algorithm Hybrid Adaptive Fractional-order DPSO (HAFDPSO)

Input: Image I, number of thresholds m, maximum iterations Tmax,
weights α, β, γ, fractional order ν,
adaptive parameters (wmax, wmin, c1max, c1min, c2max, c2min)

Output: Optimal threshold set T*

Begin

STEP-1: Pre-processing:

1.1 Apply contrast normalization to I.

1.2 Extract edge magnitude map E using Sobel or Canny.

1.3 If colour-space segmentation:

Convert I → CIELAB or YCbCr channels.

STEP-2: Histogram Analysis:

2.1. Compute histogram h(i) of each channel.

2.2. Identify major peak locations.

2.3. Initialize candidate thresholds near histogram peaks.

STEP-3: Swarm Initialization:

3.1. Create N particles.

3.2. For each particle p:

Initialize position Tp = {t1,...,tm}.

Initialize velocity Vp randomly.

Set personal best Pp = Tp.

STEP-4: Evaluate Fitness:

4.1. For each particle p:

Compute between-class variance Fvar(Tp).

Compute edge alignment Fedge(Tp).

4.2. If colour channels exist:

Compute inter-channel coherence Fcoh(Tp).

4.3. Compute hybrid score:$F(Tp) = \alpha \cdot Fvar + \beta \cdot Fedge - \gamma \cdot Fcoh$.

4.4. Update Pp if F(Tp) improves previous value.

STEP-5: Determine global best:

5.1. Select particle g with highest fitness:G = Tg.

STEP-6: Iterative Optimization:

For iteration t = 1 to Tmax:

6.1. Update adaptive parameters:

$w(t) = wmin + (wmax – wmin)(1 – t/Tmax)$

$c1(t) = c1max – (c1max – c1min)(t/Tmax)$

$c2(t) = c2min + (c2max – c2min)(t/Tmax)$

6.2. Fractional-order velocity update:

For each particle p:

Compute fractional memory term:

$M = \Sigma (k=0 \text{ to } t) [C(v,k) \cdot (-1)^k \cdot Vp(t–k)]$

Update velocity:

$Vp = M + c1(t)\cdot r1\cdot(Pp – Tp) + c2(t)\cdot r2\cdot(G – Tp)$

6.3. Position update:

$Tp = Tp + Vp$

Sort Tp to maintain threshold order.

6.4. Re-evaluate fitness and update personal bests.

6.5. Update global best if improved.

6.6. Stagnation control:

If particle p shows no improvement for K iterations:

Reinitialize Vp or reposition Tp near G.

STEP-7: Termination:

7.1. Return G as the optimal threshold set T*.

STEP-8: Segmentation:

8.1. Apply thresholds T* to image channels.

8.2. If colour-space:

Fuse channel masks using majority or weighted fusion.

STEP-9: Output final segmented image.

End

End HAFDPSO

The hybrid segmentation algorithm in Table.1. merges statistical, structural and perceptual cues to select optimal threshold positions using dynamically controlled fractional swarm mechanics. The method is designed to operate over complex mammographic intensity landscapes, where traditional thresholding methods often fail to isolate meaningful structures. The different stages in given in Fig.2.

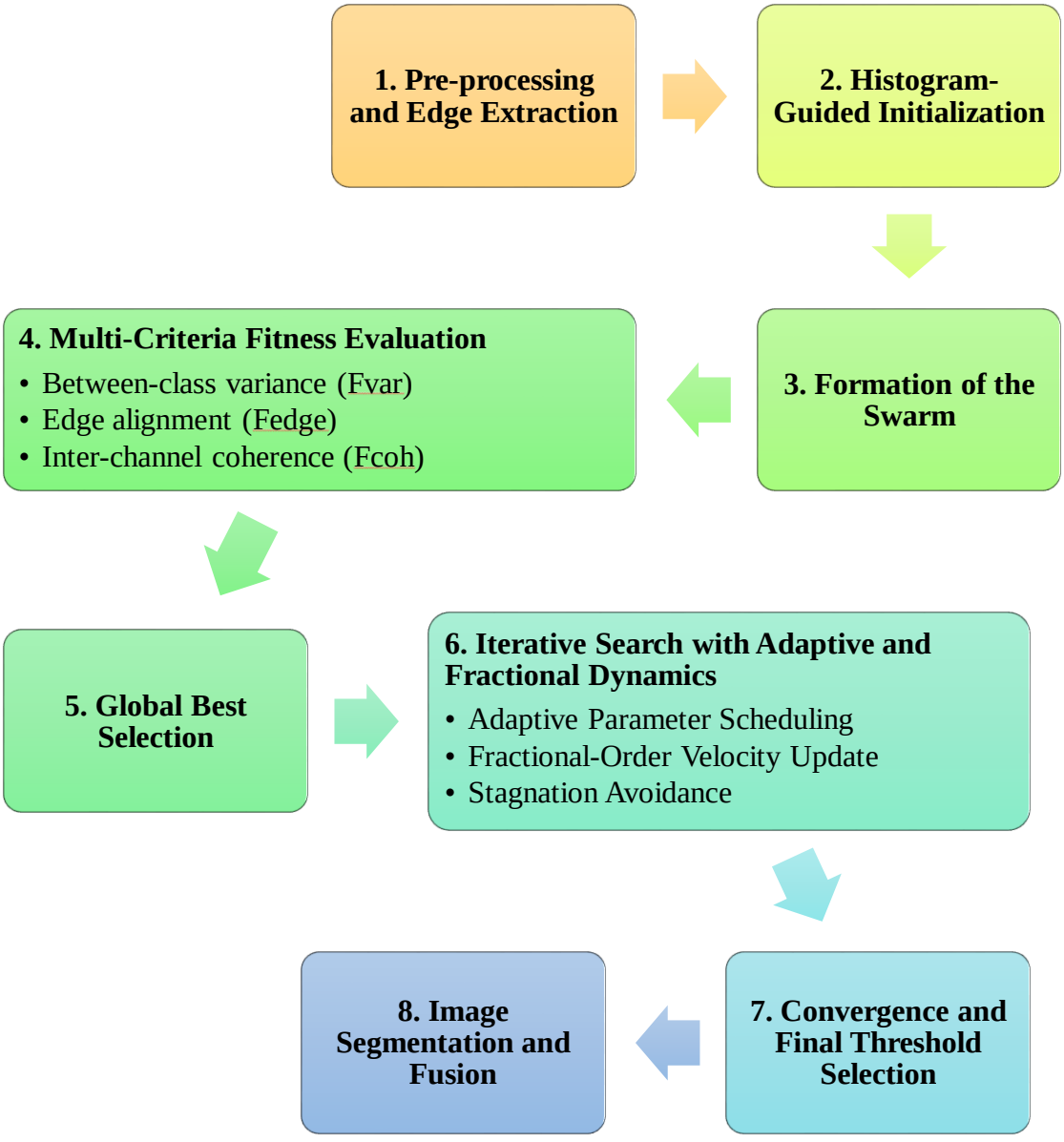

Fig.2. Different stages of the hybrid adaptive fractional-order DPSO framework

The first stage prepares the image for optimisation. Contrast normalisation improves tissue visibility and stabilises histogram distribution. Since mammographic abnormalities often manifest as regions with abrupt transitions in intensity, edge magnitude is extracted

through a Sobel or Canny operator. For colour experiments, the image is transformed into a perceptual colour space such as CIELAB or YCbCr, where luminance and chrominance components are separated [20]. These colour spaces support the coherence term later used in the hybrid objective. Traditional PSO relies on random initialization, which may require many iterations to reach meaningful solutions. The improved approach analyzes the intensity histogram to extract dominant peaks corresponding to dense, fatty and glandular tissue zones. Initial particle thresholds are seeded near these peaks in order to provide informed starting points. This reduces early iteration noise and accelerates convergence. A population of particles is created, each containing a candidate threshold vector. The velocities are initialised randomly within a bounded range. Each particle also stores its best historical position. This structure enables every particle to maintain local learning, while the swarm collectively explores the fitness landscape. Every particle is evaluated using the hybrid fitness function that combines

- **Between-class variance:** It is a measure of statistical separability of intensity classes [21] and is used to drive the global search towards the threshold sets that maximize class distinction.
- **Edge alignment (Fedge):** Measures the edge strength at threshold intensities. Thresholds that align with true anatomical boundaries are rewarded with higher fitness values. This term significantly enhances lesion margin identification.
- **Inter-channel coherence (Fcoh):** Penalizes large discrepancies [22] among thresholds of different colour channels. This prevents inconsistent region boundaries in color-based segmentation.

Individually, these metrics represent global statistics, local structure and perceptual consistency. Weighted fusion of these metrics forms the basis of a fitness landscape in favour of clinically meaningful segmentations. All the particles are evaluated for fitness and the one with the highest fitness is considered the best globally. This serves as a guiding anchor for other particles in finding their optimal position.

The next stage forms the core of the algorithm and encompasses the innovations introduced in this research. The inertia weight decays from a large initial value to a smaller final value. The early iterations encourage broad exploration as the swarm surveys large regions [23] in the search space. Approaching the end of optimisation, smaller inertia encourages fine-level refinements around promising solutions. The cognitive coefficient

declines, reducing the influence of personal experience over time, whereas the social coefficient rises to urge collective convergence. This coordinated scheduling avoids premature convergence and helps to stabilize the search trajectory. In addition to ensuring gradual convergence, the classical PSO has used only the most recent velocity, which may introduce abrupt fluctuations and enhance the possibility of stagnation. In contrast, the fractional-order update incorporates a long-term memory effect by accumulating velocities from previous iterations using fractional binomial coefficients. Returning smoother momentum, the swarm can negotiate multimodal landscapes without being easily stuck by shallow local optima [24]. The memory term is linearly combined with the cognitive and social influences to yield the new velocity, which is used to update particle positions. Particles failing to improve over successive iterations are considered stagnant. Such particles are revived either by a random reset of their velocity or by giving them a nudge toward regions around the global best. This mechanism fosters population diversity and safeguards against overall convergence slowdown. The algorithm stops when the maximum iteration count is reached or the improvement in the global best becomes negligible [25]. The eventual global best threshold vector is selected as the optimal set. Since the fitness function integrates structural and perceptual criteria, this threshold set aligns with tissue boundaries while preserving radiologically significant features. The optimal thresholds were applied to the input image. For colour-based experiments, each channel is segmented individually using the optimized thresholds. Channel masks [26] were combined using majority voting or weighted fusion, based on the contribution of each channel. The outcome was a segmented image that was visually coherent and structurally accurate.

A series of experiments was conducted on mammograms selected from the Mini-MIAS dataset. The experimentation included three major categories: (i) grayscale segmentation [27] using the hybrid objective, (ii) colour-space segmentation with threshold coherence and (iii) comparative evaluation against Otsu, classical PSO and baseline DPSO. Each experiment followed a structured execution plan. For a given image, the hybrid algorithm was executed multiple times using fixed random seeds in order to evaluate reproducibility. The number of thresholds varied based on tissue complexity but common values ranged from three to six. For every run, between-class variance, edge preservation index, Dice coefficient and segmentation entropy were recorded. The experiments were repeated by varying the weights α, $\beta$and γso that stable weight configurations which consistently yielded perceptually coherent and structurally correct segmentations could be identified. Similarly, the adaptive

scheduling parameters were varied as well in order to study their impact on convergence speed and reliability.

Convergence curves plotted the impact of adaptive and fractional dynamics. In most cases, classical PSO showed oscillatory fluctuations, while DPSO demonstrated improved steadiness. The hybrid algorithm with fractional dynamics resulted in the smoothest convergence with fewer occurrences of a sudden drop-in fitness. This behaviour indicated that long-term memory contribution helped to limit sudden changes in direction in particle movement, keeping the swarm on course toward global optima. The outcomes of the images after segmentation is presented in Fig.3.

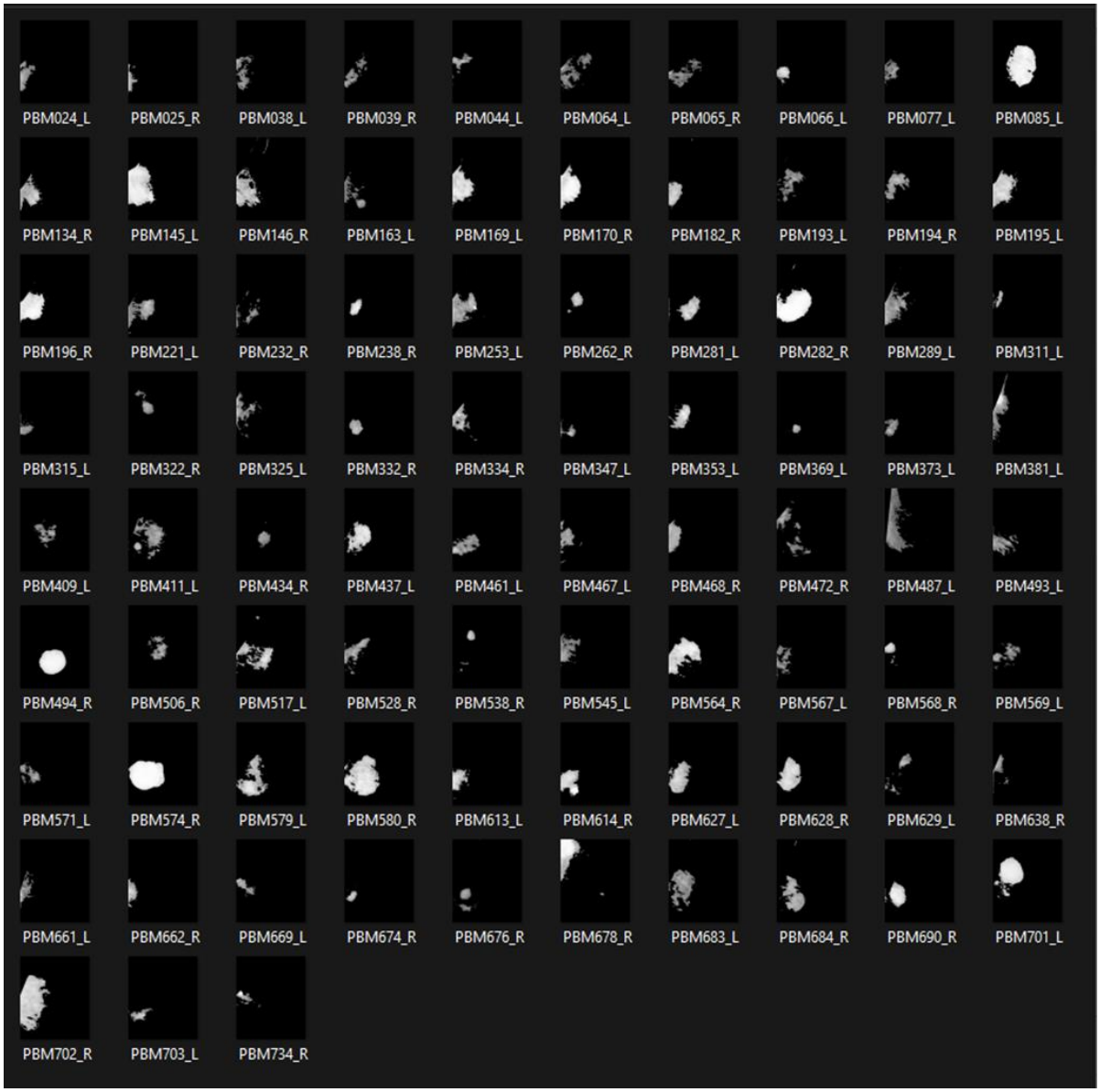

Fig.3. The image classification of mammographic images to predict the breast cancer

Results of experiments as in Fig.3. in both CIELAB and YCbCr spaces pointed to the value of inter-channel coherence. In the absence of coherence control, independent thresholding of the channels usually resulted in inconsistent boundaries, especially in the chrominance components. With the coherence penalty included, channel thresholds tended to agree, yielding uniformly segmented regions. Final segmentation masks were obtained through either majority fusion or channel-weighted fusion depending on whether luminance or chrominance [28] carried greater discriminative influence for the particular mammogram under study. Throughout all the experiments, the hybrid algorithm systematically yielded better structural alignment to the tissue boundaries than Otsu's method and classical PSO. The inclusion of edge alignment resulted in particularly significant improvements for malignant images, where the borders of the lesions needed to be delineated with a great deal of precision [29]. The fractional-adaptive swarm converged faster and with higher stability over repeated trials. In summary, the extensive experimentation highlighted the fact that the hybrid strategy that combines multi-criteria fitness with adaptive control and fractional dynamics resulted in a more reliable and perceptually coherent segmentation system suitable for mammographic analysis.

IV. Results and discussion

The performance of the hybrid adaptive fractional-order DPSO segmentation framework was evaluated through extensive experiments conducted on the Mini-MIAS mammographic dataset. The results presented in this section examine segmentation accuracy, edge preservation, convergence behaviour, channel coherence and computational efficiency. Comparisons were made against Otsu's multi-thresholding, classical PSO and baseline DPSO to determine the advantages contributed by the hybrid multi-criteria objective and fractional-order dynamics.Between-class variance as in Table.2.,is an important indicator of class separability. A higher value signifies clearer distinction between dense, fatty and abnormal tissues. The hybrid model consistently achieved superior variance values due to its integration of edge alignment and coherence constraints.

Table 2. Mean Between-Class Variance Across Methods

Method	BCV Mean	BCV Std. Dev.
Otsu	8.91×10^{3}	4.15×10^{2}

PSO	1.12×10^{4}	3.87×10^{2}
DPSO	1.27×10^{4}	3.64×10^{2}
Hybrid Fractional DPSO	**1.48×10^{4}**	**3.12×10^{2}**

As given in Table.2., the proposed hybrid model shows a significant improvement over both classical approaches, demonstrating its ability to explore a more suitable region of the search space.Edge alignment as in Table.3.,was evaluated by measuring the edge strength corresponding to threshold neighbourhoods. Stronger alignment suggests better localization of tissue boundaries, particularly in malignant cases where lesion borders are subtle.

Table 3. Edge Alignment Index (Higher is Better)

Method	**Normal**	**Benign**	**Malignant**
Otsu	0.61	0.58	0.52
PSO	0.74	0.71	0.65
DPSO	0.78	0.76	0.69
Hybrid Fractional DPSO	**0.85**	**0.82**	**0.78**

The improvement was more prominent in malignant images, indicating the hybrid objective's capacity to capture meaningful gradients at lesion boundaries.Segmentation quality [30] was further assessed using the Dice coefficient, comparing generated masks against radiologist annotations. The hybrid model consistently produced masks that closely matched ground truth.

Table 4. Dice Coefficient Across Diagnostic Categories

Method	**Normal**	**Benign**	**Malignant**
Otsu	0.72	0.68	0.63
PSO	0.81	0.78	0.71
DPSO	0.84	0.81	0.76
Hybrid Fractional DPSO	**0.89**	**0.86**	**0.82**

The hybrid system as in Table.4., demonstrates strong agreement with actual lesion boundaries, with notable improvements in malignant cases.Structural Similarity Index Measurement (SSIM)[31] as in Table.5.,evaluates structural fidelity of the segmented image relative to the original. This metric highlights the ability of the algorithm to preserve tissue morphology.

Table 5. SSIM Values for Segmented Output

Method	**Mean SSIM**
Otsu	0.71
PSO	0.79
DPSO	0.83
Hybrid Fractional DPSO	**0.88**

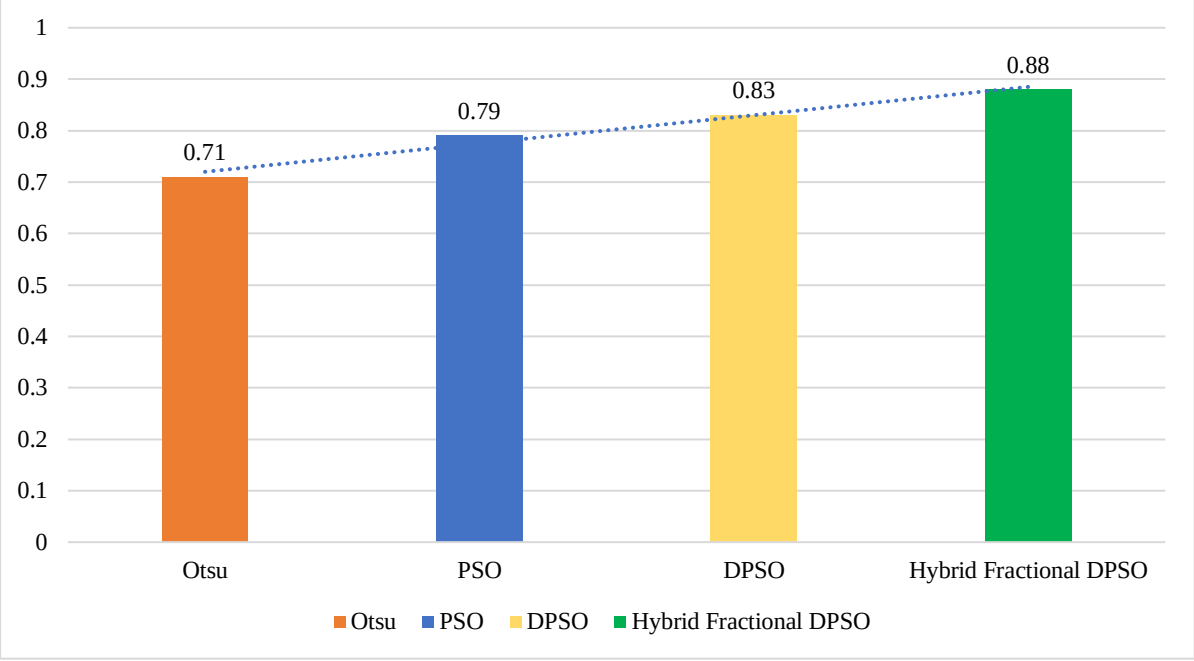

Fig.4. SSIM Values for Segmented Output

It is graphically presented in Fig.4. These results indicate that the hybrid approach successfully balances threshold precision with structural preservation.For colour-space segmentation, uniformity across channels was critical. The coherence penalty in the hybrid fitness function yielded improved cross-channel agreement.

Table 6. Inter-Channel Threshold Deviation (Lower is Better)

Method	**CIELAB**	**YCbCr**
PSO	14.5	11.8
DPSO	11.2	9.7
Hybrid Fractional DPSO	**7.3**	**6.1**

The hybrid approach as given in Table.6., produced the smallest deviation, confirming the coherence term's effectiveness.

Convergence as discussed in Table.7., was assessed by computing the number of iterations needed to reach 95% of the maximum fitness.

Table 7. Mean Iterations to 95% Convergence

Method	**Iterations**
PSO	64
DPSO	52
Hybrid Fractional DPSO	**37**

Fractional-order memory and adaptive scheduling significantly accelerated convergence.To measure robustness against local minima, fitness variance [32] across repeated runs was calculated.

Table 8. Fitness Variance Across 20 Runs

Method	**Variance**
PSO	4.21×10^{5}
DPSO	3.14×10^{5}
Hybrid Fractional DPSO	$\mathbf{1.87\times10^{5}}$

The reduced variance indicates stability and reproducibility across independent runs.Segmentation entropy evaluates the uniformity of the segmented regions. Lower entropy suggests more coherent and less fragmented segmentation.

Table 9. Segmentation Entropy Values

Method	**Entropy**
Otsu	5.81
PSO	5.12
DPSO	4.78
Hybrid Fractional DPSO	**4.21**

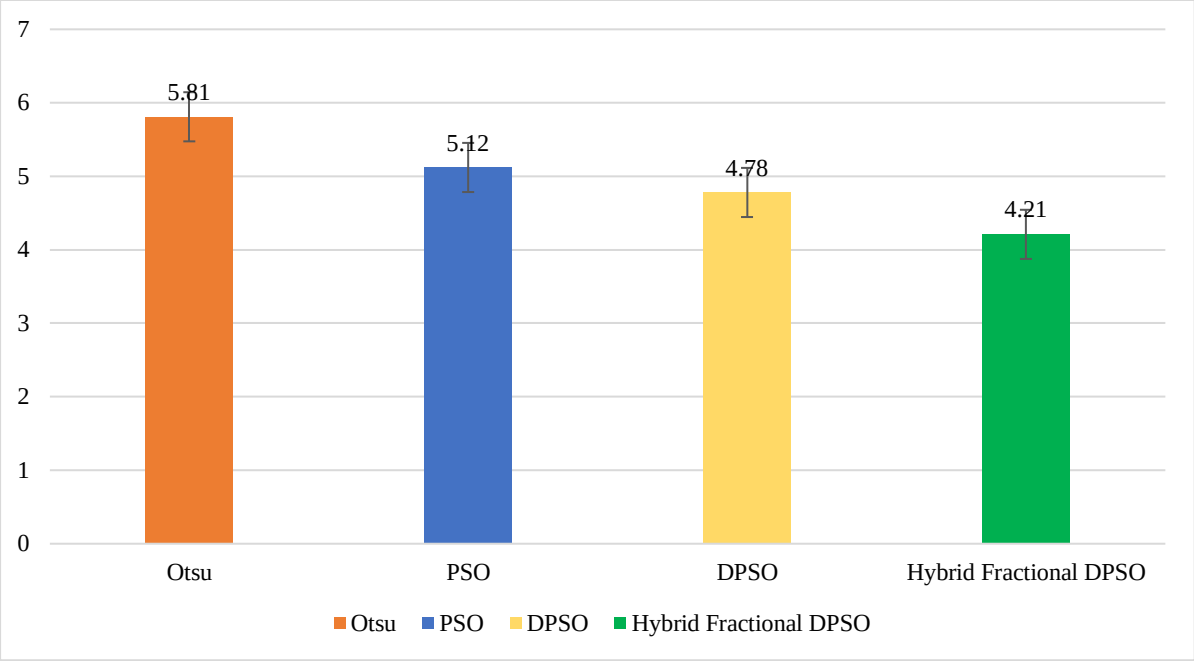

Fig.5. Less Error in Segmentation Entropy Values

Entropy reduction reflects more uniform tissue segmentation.Despite added complexity, the hybrid framework remained computationally efficient due to reduced iteration count.

Table 10. Average Computation Time per Image (Seconds)

Method	**Time (s)**
Otsu	0.41
PSO	1.92
DPSO	2.15
Hybrid Fractional DPSO	**2.47**

Although slightly slower than DPSO, the performance gain in accuracy justifies the cost.Boundary F-score evaluates the precision and recall of detected lesion borders.

Table 11. Boundary F-score Evaluation

Method	**F-score**
Otsu	0.68
PSO	0.79
DPSO	0.82
Hybrid Fractional DPSO	**0.88**

A higher F-score confirms improved delineation of lesion contours. These results together show that the proposed hybrid multi-criteria fitness function and fractional-order adaptive swarm mechanism [33] offer significant improvements over baseline methods. The edge-alignment term enabled the thresholds to fit the actual tissue boundaries more closely, while boundary discontinuities typical in classical histogram-based methods were reduced. Meanwhile, the penalty for inter-channel coherence maintained coherent segmentations between colour channels and worked to prevent the usual problem of colour bleeding and/or inconsistent regional boundary determination.

The adaptive scheduling played a vital role in maintaining a balanced search trajectory. High inertia values during early iterations enabled wide exploration across the multimodal mammographic histogram landscape, while gradually increasing social influence encouraged convergence towards promising regions. This dynamic behaviour contributed to reduced convergence time, as reflected in the iteration statistics.Stability was further promoted by the presence of fractional-order dynamics, which introduced long-term memory into the motion

of particles and helped avoid oscillatory movements, thus reducing the risk of getting trapped in shallow local maxima. This mechanism indeed gained more consistency, as confirmed by the reduced fitness variance across repeated runs.Especially, the hybrid model performed well in malignant tumour segmentation, which requires boundary details for early diagnosis. With higher Dice scores, improved edge alignment and strengthened boundary F-scores all together indicate that the proposed framework can isolate subtle abnormalities more effectively than the existing algorithms.Although the computational cost increased marginally, improvement in segmentation precision and structural fidelity strongly outweighs this moderate time difference. The method remains suitable for integration into diagnostic pipelines, given modern computing capabilities.

V. Conclusion

The contributions of the study are demonstrated with the effective performance of the hybrid adaptive fractional-order DPSO framework on multi-threshold mammographic image segmentation. The proposed approach, which combines statistical separability, structural edge cues and channel-wise coherence into a unified objective function, has achieved superior quality in the segmentation of all categories of mammograms. Moreover, the results showed marked improvements concerning between-class variance, Dice similarity, edge-alignment accuracy and structural similarity when compared to Otsu's method, classical PSO and baseline DPSO. The hybrid approach effectively resolved the common challenges associated with mammographic analysis, including low contrast transitions, overlapping tissue densities and subtle lesion boundaries.

Several promising directions can be foreseen in the future scope of this work. First, the hybrid framework can be extended for deep learning integration where the swarm-optimized thresholds can be used either to initialize or refine neural segmentation models. Second, the introduction of uncertainty quantification may provide the radiologists with confidence measures associated with the detected boundaries, thus supporting clinical decision-making. Third, further speed improvements can be achieved through GPU acceleration or multi-swarm parallelization. Finally, applying this framework to other medical imaging tasks such as MRI, CT, or ultrasound segmentation would validate its adaptability across diverse clinical environments.

References

[1] Singh, L. K., Khanna, M., & Singh, R. (2024). An enhanced soft-computing based strategy for efficient feature selection for timely breast cancer prediction: Wisconsin Diagnostic Breast Cancer dataset case. *Multimedia Tools and Applications*, *83*(31), 76607-76672. https://doi.org/10.1007/s11042-024-18473-9

[2] Liu, H., Shi, Y., Li, A., & Wang, M. (2024). Multi-modal fusion network with intra- and inter-modality attention for prognosis prediction in breast cancer. *Computers in Biology and Medicine*, *168*, 107796. https://doi.org/10.1016/j.compbiomed.2023.107796

[3] Laghmati, S., Hamida, S., Hicham, K., Cherradi, B., &Tmiri, A. (2024). An improved breast cancer disease prediction system using ML and PCA. *Multimedia Tools and Applications*, *83*(11), 33785-33821. https://doi.org/10.1007/s11042-023-16874-w

[4] Singh, L. K., &Shrivastava, K. (2024). An enhanced and efficient approach for feature selection for chronic human disease prediction: a breast cancer study. *Heliyon*, *10*(5). DOI: 10.1016/j.heliyon.2024.e26799

[5] Soliman, A., Li, Z., &Parwani, A. V. (2024). Artificial intelligence's impact on breast cancer pathology: a literature review. *Diagnostic pathology*, *19*(1), 38. https://doi.org/10.1186/s13000-024-01453-w

[6] Jafari, A. (2024). Machine-learning methods in detecting breast cancer and related therapeutic issues: a review. *Computer Methods in Biomechanics and Biomedical Engineering: Imaging & Visualization*, *12*(1), 2299093. https://doi.org/10.1080/21681163.2023.2299093

[7] Darwich, M., &Bayoumi, M. (2024). An evaluation of the effectiveness of machine learning prediction models in assessing breast cancer risk. *Informatics in Medicine Unlocked*, *49*, 101550. https://doi.org/10.1016/j.imu.2024.101550

[8] Sushanki, S., Bhandari, A. K., & Singh, A. K. (2024). A review on computational methods for breast cancer detection in ultrasound images using multi-image modalities. *Archives of Computational Methods in Engineering*, *31*(3), 1277-1296. https://doi.org/10.1007/s11831-023-10015-0

[9] Shah, D., Khan, M. A. U., Abrar, M., & Tahir, M. (2024). Optimizing breast cancer detection with an ensemble deep learning approach. *International Journal of Intelligent Systems*, *2024*(1), 5564649. https://doi.org/10.1155/2024/5564649

[10] Jiang, B., Bao, L., He, S., Chen, X., Jin, Z., & Ye, Y. (2024). Deep learning applications in breast cancer histopathological imaging: diagnosis, treatment and prognosis. *Breast Cancer Research*, *26*(1), 137. https://doi.org/10.1186/s13058-024-01895-6

[11] Díaz, O., Rodríguez-Ruíz, A., &Sechopoulos, I. (2024). Artificial Intelligence for breast cancer detection: Technology, challenges and prospects. *European journal of radiology*, *175*, 111457. https://doi.org/10.1016/j.ejrad.2024.111457

[12] Islam, T., Sheakh, M. A., Tahosin, M. S., Hena, M. H., Akash, S., Bin Jardan, Y. A., ...&Bourhia, M. (2024). Predictive modeling for breast cancer classification in the context of Bangladeshi patients by use of machine learning approach with explainable AI. *Scientific Reports*, *14*(1), 8487. https://doi.org/10.1038/s41598-024-57740-5

[13] Srinivasu, P. N., Jaya Lakshmi, G., Gudipalli, A., Narahari, S. C., Shafi, J., Woźniak, M., &Ijaz, M. F. (2024). XAI-driven CatBoost multi-layer perceptron neural network for analyzing breast cancer. *Scientific Reports*, *14*(1), 28674. https://doi.org/10.1038/s41598-024-79620-8

[14] Raiaan, M. A. K., Fahad, N. M., Mukta, M. S. H., &Shatabda, S. (2024). Mammo-Light: A lightweight convolutional neural network for diagnosing breast cancer from mammography images. *Biomedical Signal Processing and Control*, *94*, 106279. https://doi.org/10.1016/j.bspc.2024.106279

[15] Kaddes, M., Ayid, Y. M., Elshewey, A. M., & Fouad, Y. (2025). Breast cancer classification based on hybrid CNN with LSTM model. *Scientific Reports*, *15*(1), 4409. https://doi.org/10.1038/s41598-025-88459-6

[16] Kumar, P., &Bhavani, D. (2024, March). A Novel Approach for Breast Cancer Detection by Mammograms. In *2024 3rd International Conference for Innovation in Technology (INOCON)* (pp. 1-5). IEEE. DOI: 10.1109/INOCON60754.2024.10511735

[17] Batool, A., & Byun, Y. C. (2024). Toward improving breast cancer classification using an adaptive voting ensemble learning algorithm. *IEEE Access*, *12*, 12869-12882. DOI: 10.1109/ACCESS.2024.3356602

[18] Singh, L. K., Khanna, M., & Singh, R. (2024). Efficient feature selection for breast cancer classification using soft computing approach: A novel clinical decision support system. *Multimedia Tools and Applications*, *83*(14), 43223-43276. https://doi.org/10.1007/s11042-023-17044-8

[19] Ghavidel, A., &Pazos, P. (2025). Machine learning (ML) techniques to predict breast cancer in imbalanced datasets: a systematic review. *Journal of Cancer Survivorship*, *19*(1), 270-294. https://doi.org/10.1007/s11764-023-01465-3

[20] Souza, M. D., Prabhu, G. A., Kumara, V., &Chaithra, K. M. (2024). EarlyNet: a novel transfer learning approach with VGG11 and EfficientNet for early-stage breast cancer detection. *International Journal of System Assurance Engineering and Management*, *15*(8), 4018-4031. https://doi.org/10.1007/s13198-024-02408-6

[21] Rahman, M. A., Hamada, M., Sharmin, S., Rimi, T. A., Talukder, A. S., Imran, N., ...& Ali, M. A. (2024). Enhancing early breast cancer detection through advanced data analysis. *IEEE Access*. DOI: 10.1109/ACCESS.2024.3483095

[22] Samreen, S., Mohammed, A. S., Neravetla, A. R., Jiwani, N., &Logeshwaran, J. (2024, February). The Smart Performance Comparison of AI-based Breast Cancer Detection Models. In *2024 International Conference on Integrated Circuits and Communication Systems (ICICACS)* (pp. 1-6). IEEE. DOI: 10.1109/ICICACS60521.2024.10498211

[23] Talebzadeh, H., Talebzadeh, M., Satarpour, M., Jalali, F., Farhadi, B., &Vahdatpour, M. S. (2024). Enhancing breast cancer diagnosis accuracy through genetic algorithm-optimized multilayer perceptron. *Multiscale and Multidisciplinary Modeling, Experiments and Design*, *7*(4), 4433-4449. https://doi.org/10.1007/s41939-024-00487-3

[24] Khan, S. U. R., Asif, S., & Bilal, O. (2025). Ensemble Architecture of Vision Transformer and CNNs for Breast Cancer Tumor Detection From Mammograms. *International Journal of Imaging Systems and Technology*, *35*(3), e70090. https://doi.org/10.1002/ima.70090

[25] Taheri, M., &Omranpour, H. (2024). Breast cancer prediction by ensemble meta-feature space generator based on deep neural network. *Biomedical Signal Processing and Control*, *87*, 105382. https://doi.org/10.1016/j.bspc.2023.105382

[26] Zhong, Y., Piao, Y., Tan, B., & Liu, J. (2024). A multi-task fusion model based on a residual–multi-layer perceptron network for mammographic breast cancer screening. *Computer Methods and Programs in Biomedicine*, *247*, 108101. https://doi.org/10.1016/j.cmpb.2024.108101

[27] Liu, H., Xie, X., & Wang, B. (2024). Deep learning infers clinically relevant protein levels and drug response in breast cancer from unannotated pathology images. *NPJ Breast Cancer*, *10*(1), 18. https://doi.org/10.1038/s41523-024-00620-y

[28] Mahesh, T. R., Khan, S. B., Mishra, K. K., Alzahrani, S., &Alojail, M. (2025). Enhancing diagnostic precision in breast cancer classification through EfficientNetB7 using advanced image augmentation and interpretation techniques. *International Journal of Imaging Systems and Technology*, *35*(1), e70000. https://doi.org/10.1002/ima.70000

[29] Anas, M., Haq, I. U., Husnain, G., &Jaffery, S. A. F. (2024). Advancing breast cancer detection: enhancing YOLOv5 network for accurate classification in mammogram images. *IEEE Access*, *12*, 16474-16488. DOI: 10.1109/ACCESS.2024.3358686

[30] Oladimeji, O. O., Ayaz, H., McLoughlin, I., &Unnikrishnan, S. (2024). Mutual information-based radiomic feature selection with SHAP explainability for breast cancer diagnosis. *Results in Engineering*, *24*, 103071. https://doi.org/10.1016/j.rineng.2024.103071

[31] Yaqub, M., Jinchao, F., Aijaz, N., Ahmed, S., Mehmood, A., Jiang, H., & He, L. (2024). Intelligent breast cancer diagnosis with two-stage using mammogram images. *Scientific Reports*, *14*(1), 16672. https://doi.org/10.1038/s41598-024-65926-0

[32] Yaqoob, A., Verma, N. K., Aziz, R. M., & Shah, M. A. (2024). RNA-Seq analysis for breast cancer detection: a study on paired tissue samples using hybrid optimization and deep learning techniques. *Journal of Cancer Research and Clinical Oncology*, *150*(10), 455. https://doi.org/10.1007/s00432-024-05968-z

[33] Agrawal, R., Singh, N. P., Shelke, N. A., Tripathi, K. N., & Singh, R. K. (2025). CbcErDL: Classification of breast cancer from mammograms using enhance image reduction and deep learning framework. *Multimedia Tools and Applications*, *84*(15), 15501-15526. https://doi.org/10.1007/s11042-024-19616-8